

Measurement of the $^{20-22}\text{Ne } ^3\text{P}_2\text{--}^3\text{D}_3$ transition isotope shift using a single, phase modulated laser beam

B. Ohayon, G. Gumpel, and G. Ron

Racah Inst. of Physics

(Dated: September 23, 2016)

We develop a simple technique to accurately measure frequency differences between far lying resonances in a spectroscopy signal using a single laser. This technique was used to measure the isotope shift of the cooling transition of metastable neon for the result of 1626.264(79) MHz. The most accurate determination of this value to date.

I. INTRODUCTION

Accurate measurements of atomic or molecular optical transitions usually requires overcoming the large - typically few GHz - Doppler broadening of the lines, caused by the thermal velocity distribution of the atoms.

To this end there exist a multitude of experimental methods relying on either cooling (and/or trapping) of the sample, or limiting the interaction with probing fields to a specific, narrow velocity group. The latter method is generally called Doppler-free spectroscopy (DFS) [1]. Both of these methods result in narrow lines, typically few MHz for optical transitions, which can be probed with a narrowband laser beam.

Whereas atomic-beam or trap setups require an elaborate vacuum system and sensitive detection for small observed signals, DFS of a thermal sample can be done on an optical table with a thermal gas sample in a cell, and enjoys large signal to noise ratio. Moreover, adding a discharge (AC or DC) to the cell enables spectroscopy of transitions from states besides ground or metastable. Finally, the systematic uncertainties in a vapor cell configuration are inherently different from those of cold atoms or ions, and so in some cases, both methods are used [2–4].

An accurate determination of the width and location of an atomic resonance, requires calibration of the laser wavelength within the scanning range [5]. A common way to achieve this is by using a cavity with known free-spectral-range (FSR) [6], which adds frequency markers in the form of narrow resonances whenever the laser is scanned over the FSR. This method is limited by the uncertainty and drifts in the FSR, mostly due to thermal changes in the cavity length. Also, to account for non-linearity in the scanning procedure, many close markers are desired [7], which require long cavities, that are more susceptible to thermal drifts.

A more elaborate method of calibrating the wavelength is to phase-lock a scan laser to a reference laser locked to a stable feature, and measure their frequency difference. This method is limited by their noise, and the stability of the reference laser frequency during a measurement sequence. Higher stability is obtained when locking both lasers to a frequency comb [8], at the expense of a more elaborate and involved system.

We present simple, versatile measurement scheme

which overcomes most calibration challenges and drift errors, while using a single, unlocked laser. This method is used to measure the isotope shift (IS) of the $^3\text{P}_2 \leftrightarrow ^3\text{D}_3$ ($\lambda = 640.2$ nm) transition between ^{20}Ne and ^{22}Ne . A closed and isolated transition used for laser-cooling applications [9].

II. EXPECTED AND OBSERVED SIGNALS

A. Frequency calibration signal

A laser beam of amplitude E_0 , phase-modulated with frequency ω_m , can be described as a series of sidebands around the fundamental frequency Ω :

$$\frac{E(\Omega, t)}{E_0} = \sum_{a=-\infty}^{\infty} J_a[m] \cos[\Omega_a t], \quad (1)$$

with J_a the Bessel function of order a , m the modulation index, and $\Omega_a = \Omega - a \cdot \omega_m$ the sideband frequency. When propagated through a Fabri-Pérot (FP) interferometer with a resonance at Ω_{FP} , a free spectral range ω_{FSR} , much larger than the modulation frequency, and finesse F , the transmitted intensity can be written as [10]

$$\frac{I(\Omega)}{I_0} = \sum_{a=-\infty}^{\infty} J_a^2 L[\Omega_a - \Omega_{FP}, \omega_{FSR}/F], \quad (2)$$

where we define a normalized Lorentzian transmission function $L[\delta, \gamma] = \frac{1}{1+4(\delta/\gamma)^2}$, with full width at half max γ , detuning δ , and after filtering out terms oscillating at $a \cdot \omega_m$ for $a > 0$. Eq. 2 describes a series of Lorentzians, one for each sideband, separated by the modulation frequency. The actual signal is shown in Fig. 2 and 3.

B. Atomic signal

We implement DFS by means of saturated absorption [11]. For a single transition with resonance frequency Ω_r , and a homogeneously broadened linewidth Γ , the

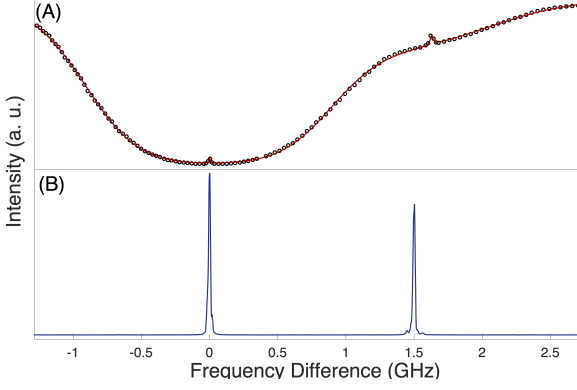


FIG. 1. Wide scan of laser frequency without phase modulations. (A) SA signal (circles), fitted with Eq. 5 (solid line). Both ^{20}Ne (left) and the less abundant ^{22}Ne (right) Gaussian dips, and narrow Doppler-free peaks are observed. (B) FP signal for calibration of frequency axis.

transmission coefficient of a weak probe beam is well-approximated in the Doppler limit by [12]

$$\frac{I(\Delta)}{I_0} = e^{-G[\Delta](1-S \cdot L[\Delta, \Gamma])}, \quad (3)$$

with G the Doppler broadened, Gaussian absorption coefficient of the atomic vapor, including the atomic density and cell length, S is the resonance depth, which depends on the pump and probe intensities, and $\Delta = \Omega - \Omega_r$ is the detuning from resonance.

For a sample containing two isotopes with an isotope shift of ω_{IS} , the transmission can be written as

$$\frac{I(\Delta)}{I_0} = e^{-G_1(1-S_1 \cdot L_1) - G_2(1-S_2 \cdot L_2)} \quad (4)$$

where, assuming that the transition in both isotopes has similar linewidth and mass, $L_2[\Delta] = L_1[\Delta - \omega_{IS}] = L[\Delta - \omega_{IS}, \Gamma]$, $G_2[\Delta] = G_1[\Delta - \omega_{IS}] \cdot n_2/n_1 = G[\Delta - \omega_{IS}] \cdot n_2/n_1$, and we suppress notation of the frequency dependencies, n_1, n_2 are the isotopic atomic densities. We expand the intensity of Eq. 4 in $G_i S_i$ to get

$$\frac{I(\Delta)}{I_0} = e^{-G_1 - G_2} (1 + G_1 S_1 L_1 + G_2 S_2 L_2 + O[(G_i S_i)^2]). \quad (5)$$

A trace of a broad frequency scan of the SA signal, fitted with Eq. 5, is shown in Fig. 1.

When the pump beam is amplitude modulated with a frequency $\omega_c \ll \Gamma$ [6, 7], the resonance depths are modulated as: $S_i \rightarrow S_i \cos(\omega_c t + \phi)$. When the absorption signal is fed into a phase sensitive amplifier, locked to the modulation frequency, this in-phase *lock-in* signal simplifies to

$$V[\Delta] \propto \alpha_1 L_1 + \alpha_2 L_2 + O[(G_i S_i)^3], \quad (6)$$

where we evaluate the absorption coefficients on resonance: $\alpha_1 = e^{-G_1[0] - G_2[-\omega_{IS}]} G_1[0] S_1$, and $\alpha_2 =$

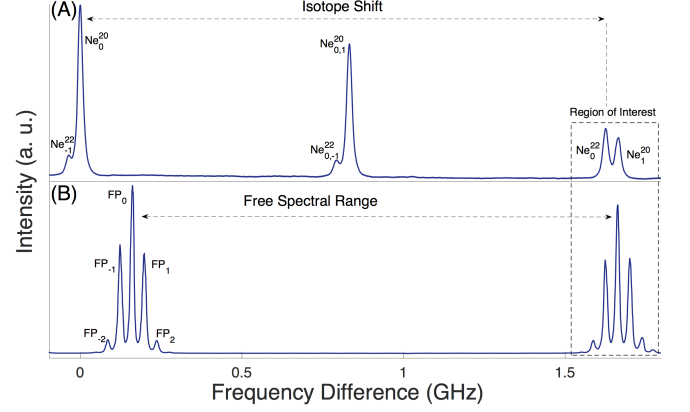


FIG. 2. Wide scan of laser frequency with phase modulations. (A) SA Lock-in signal, with $\omega_c = 4$ kHz, $\omega_M = 1.7$ GHz. Ne_a^X denotes the a sideband of isotope X . Crossovers between sidebands a, a' are denoted $\text{Ne}_{a,a'}^X$. (B) FP signal with $\omega_m = 40$ MHz. The FSR, and sidebands are denoted.

$e^{-G_1[\omega_{IS}] - G_2[0]} G_2[0] S_2$. Eq. 6 describes two Loreznians on a flat background, separated by the isotope shift, with third order nonlinear corrections to the small peak amplitudes.

We now add phase modulation with a frequency much higher than the lock-in frequency $\omega_M \gg \omega_c$, the resulting lock-in signal becomes:

$$V[\Delta] \propto \sum_{a=-\infty}^{\infty} J_a^2 (\alpha_{1,a} L_{1,a} + \alpha_{2,a} L_{2,a}) + \sum_{a \neq b} J_a J_b (\alpha_{1,ab} L_{1,ab} + \alpha_{2,ab} L_{2,ab}), \quad (7)$$

with the sideband Loreznians $L_{i,a}[\Delta] = L_i[\Delta - a \cdot \omega_M]$. Since they are independent of the laser frequency, we do not write the expressions for the peak amplitudes $\alpha_{i,k}$ explicitly. The second term in Eq. 7 represents crossover peaks for each isotope obtained when the atoms are pumped by one sideband, and probed by another, $L_{i,ab}[\Delta] = L_i[\Delta - (a+b) \cdot \omega_M/2]$. There are no crossover peaks between different isotopes. Fig. 2 shows the atomic signal presented in Eq. 7, we notice that the crossovers either fall between the atomic peaks or add to the original peaks.

When scanning the laser beam close to the second isotope resonance $\Delta \approx \omega_{IS}$, and for a modulation frequency close to the isotope shift, $\omega_M \approx \omega_{IS}$ (region of interest in Fig. 2), only two peaks survive, which are separated by the difference between the modulation frequency and the isotope shift

$$V[\Delta] \propto J_1^2 \alpha_{1,1} L[\Delta - \omega_M] + J_0^2 \alpha_{2,0} L[\Delta - \omega_{IS}]. \quad (8)$$

Fig. 3 shows the Lock-in signal in the region of interest, fitted with Eq. 8, along with the frequency calibration signal, fitted with Eq. 2.

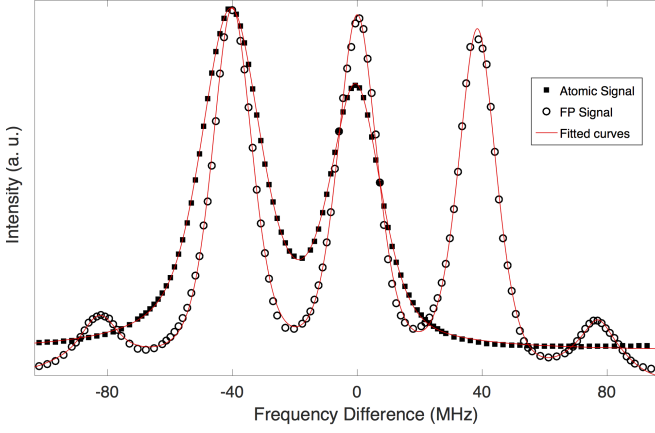


FIG. 3. Narrow scan of the region of interest (see Fig. 2 for a wider scan), with typical EOM frequencies $\omega_m = 40$ MHz and $\omega_M = 1666$ MHz. Circle markers correspond to the atomic signal from the lock-in amplifier, fitted with Eq. 8. Full squares correspond to FP signal, fitted with Eq. 2.

III. EXPERIMENTAL REALIZATION

A. Setup

We use a narrow-band single frequency laser beam, from a home-built external cavity diode laser (ECDL) [13]. Frequency scanning is performed by applying voltage to a piezoelectric element connected to the external cavity. The beam is split in two using a polarizing beam splitter. One beam goes through a broadband, low frequency (DC-100 MHz) commercial electro-optic-modulator (EOM, New Focus 4002) and into a Fabri-Pérot cavity (Thorlabs SA-200, $\omega_{FSR} = 1.5$ GHz, $F = 200$). The other beam goes through a home-built, narrowband, high frequency EOM [14], and enters a pump-probe type saturated absorption setup with natural abundance neon gas (90% Ne^{20} , 9% Ne^{22} and 0.3% Ne^{21}) at 200 mTorr, contained in a sealed, anti-reflection coated, glass cell. The cell resides in a high-Q coaxial resonator chamber [15]. An rf-driven discharge at the resonance frequency (70.4 MHz) excites the atoms and populates higher lying states [16]. After ignition, a few milliwatts of RF-power are sufficient to maintain stable plasma.

The SA setup consists of collinear pump and probe beams to avoid angle-dependent systematic shifts [2]. The pump beam is amplitude modulated by a chopper at 4 kHz. A reference beam goes through the cell as well, and provides another stage of subtraction to remove amplitude noise in the laser and discharge from the signal. The signal is fed into a lock-in amplifier (SRS SR830) where it is mixed with the chopper reference, filtered and amplified. Fig. 4 shows the main elements of the experimental system.

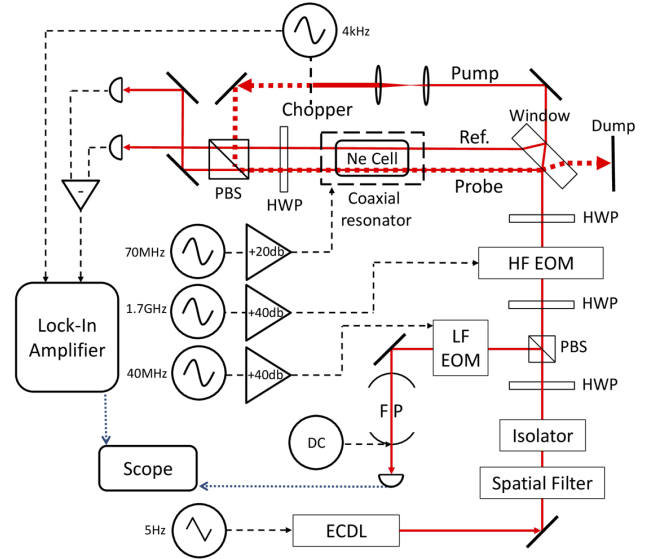


FIG. 4. Main elements of optical and electronic setup. EOM - Electro-optic modulator, HF - High frequency, LF - Low frequency, HWP - Half wave plate. FP - Fabri-Pérot interferometer, ECDL - External cavity diode laser, PBS - Polarizing beam splitter.

B. Sequence

A slow (few Hz) and narrow scan of the laser frequency results in traces of the lock-in and FP signals simultaneously (Fig. 2 and 3). We tune the relative FP frequency position by applying DC voltage to a piezoelectric element moving one of the cavity mirrors. From Eq. 8, the distance between the zero-order ^{22}Ne peak and the first-order ^{20}Ne is exactly $\omega_d = \omega_M - \omega_{IS}$. We tune the low-frequency EOM to $\omega_m \approx \omega_d$ by placing two of the FP sideband peaks directly on top of the lock-in atomic signal peaks (see Fig. 3). This limits the effects of scan nonlinearity in calibration of the frequency axis to less than a few kHz. To each trace we fit the atomic signal with two Lorentzians of Eq. 8, and the FP signal with five Lorentzians corresponding to the $0, \pm 1, \pm 2$ sideband orders observed (Eq. 2). To account for non-homogeneous broadening, and so model the tails of the peaks accurately, each Lorentzian in the fits is replaced with a pseudo-Voigt profile [17].

The fitting procedure gives the distances between the FP peaks τ_{FP} and the Atomic peaks τ_{LI} in units of time, and so the isotope shift is calculated as:

$$\omega_{IS} = \omega_M - \omega_d = \omega_M - \omega_m \tau_{LI} / \tau_{FP}. \quad (9)$$

This procedure of obtaining the IS is robust against frequency drifts in the laser, since both the atomic and FP signals drift together. The FP FSR is not used, and so slow (few minutes) thermal drifts in the cavity length only serve to move the FP signal relative to the atomic signal.

The results of each experimental run are calculated

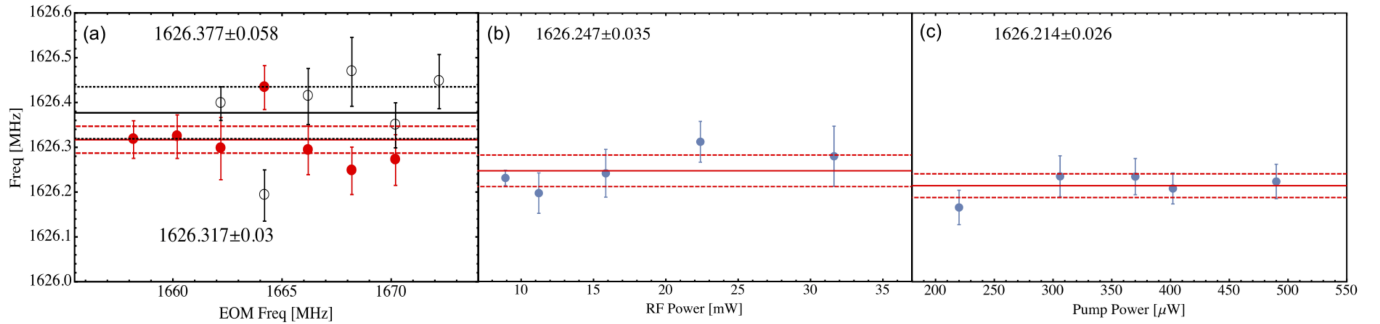


FIG. 5.

Calculated isotope shift frequency when varying experimental parameters. (a) Changing both EOM frequencies (see text). Horizontal axis labeled by the narrowband EOM frequency. Full circles are at 10 mW RF power and empty circles are at 30 mW. (b) Changing RF power. (c) Changing pump laser power.

using Eq. 9, and averaged using a Bayesian analysis with the JAGS [18, 19] framework. Which takes into account possible correlations between measurement errors and their intrinsic scatter.

To account for unknown systematic effects we investigate the calculated IS for different experimental parameters. By varying the laser power (Fig. 5c), we change the width of the peaks through saturation broadening [11], the power may also affect the peak location through AC stark shifts [4]. By varying the RF-discharge power (Fig. 5b), we change the excited-state population and peak height, as well as shifts which may result from non-thermal distribution of the gas sample. Hysteretic effects were observed at high RF power, where coupling of the radio-waves to the plasma changed from capacitive to inductive [20], and so we limited our investigation to low powers. The most stringent test for our measurement scheme is to vary both EOM frequencies together (Fig. 5a). This changes both the distance and magnitude of all peaks involved.

IV. RESULT AND CORRECTIONS

The results of Fig. 5 are combined using the JAGS framework to obtain 1626.288(76) MHz, where the quantity in brackets is the total uncertainty. We estimate the significance and donation of some known systematic corrections to the obtained experimental value. We note here that due to our measurement scheme, the ^{22}Ne peak appears at a lower laser frequency than the ^{20}Ne peak (See Fig. 2).

Due to their similar electronic configuration and identical quantum numbers, most of the systematic shifts between the lines of ^{20}Ne and ^{22}Ne vanish to high orders when measuring the isotope shift. Among those are Zeeman shifts. The 3P_2 and 3D_3 levels in neon are 24THz and 5THz apart from their closest neighbors respectively. Since quantum interference shift is inversely proportional to the difference between the levels [21], this effect is vanishingly small in our case.

Naturally, the main difference between the two isotopes is their mass M . It affects the atomic recoil to create the so-called recoil shift of $\omega_r = h/(2M\lambda^2)$, a -2.2 kHz shift of the IS. The thermal distribution cancels first order Doppler shifts but adds a second order shift of $-4T/(\lambda c \pi M)$ [11], a negligible 75 Hz correction.

The mass difference affects the most probable velocity $\bar{v} = \sqrt{(2k_B T)/M}$ as well, which in turn donates to the pressure shift discussed next.

The interaction potential between neighboring atoms shifts their energy levels. In the case of a vapor cell with a small fraction of light metastables, it stems mostly from binary elastic collisions with ground state atoms [2]. for low pressures, these interactions cause broadening and shift of spectral lines by

$$\gamma_r = n\bar{v}\sigma_r, \quad (10)$$

with $n \propto P$ the ground-state density, P the cell pressure, σ_r the relevant cross-section, and $r = \{s, b\}$ for shifting and broadening collisions respectively [11].

We measured the pressure broadening at room temperature in ^{20}Ne to be $\gamma_b = 11 \pm 1$ MHz/Torr. This value lies in between the measured (11.8 ± 0.9 to 12.8 ± 0.8 MHz) and calculated (9.5 to 9.8 MHz) values for similar transitions in neon from the same ground state [22]. Repeating the measurement for ^{22}Ne we get 10.5 ± 0.7 MHz/Torr. Plugging the measured broadening to Eq. 10, we get that the broadening cross-sections for the two isotopes at room temperature are within uncertainties: $\sigma_b^{22}/\sigma_b^{20} = 1.0 \pm 0.1$.

For the shift, Leo *et. al.* reports $\gamma_s = -1.9$ to -2.1 MHz/Torr for similar transitions at room temperature neon [22]. Following the similarity in broadening we assume the shift in the cooling transition is of the same order of magnitude, and that the relative cross sections for shift in the two isotopes are similar ($\sigma_s^{22}/\sigma_s^{20} \approx \sigma_b^{22}/\sigma_b^{20}$). Thus, we estimate the contribution of the linear shift to the isotope shift to be -20 ± 20 kHz for 200 mTorr.

A combination of pressure, recoil, and Doppler effects results in light-pressure shifts. The recoil of the atoms

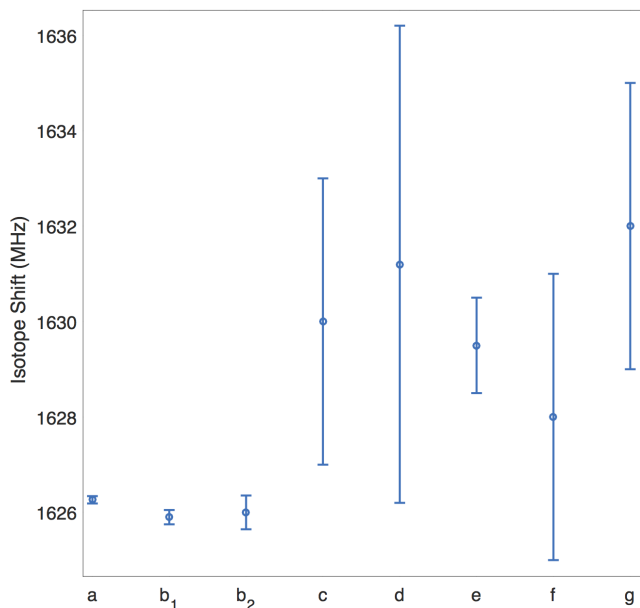


FIG. 6. Isotope shift and uncertainties obtained by different groups: (a) This work, (b) Feldker *et. al.* [24], 1 - Absorption, 2 - Fluorescence, (c) Julien *et. al.* [25], (d) Guthöhrlein *et. al.* [26], (f) Basar *et. al.* [27], (g) Odintsov *et. al.* [28].

from the pump beam creates a non-thermal velocity distribution which adds a small dispersive signal to the line-shape. Since collisions rethermalize the sample, this effect decreases at high pressure. At low saturation, the strength of this effect is independent of laser power, and manifest itself as a shift of $\omega_r \Gamma / (2\gamma_b)$ [23], which is cal-

culated for our case using the pressure broadening of Eq. 10 to be -2.2 kHz at 200 mTorr.

The corrected result for the isotope shift is 1626.264(79) MHz.

V. CONCLUSION AND OUTLOOK

We presented a simple measurement scheme for accurate determination of intervals between far (up to few GHz) lying resonances in a spectroscopy signal. This method was used to measure the isotope shift between the ^{20}Ne and ^{22}Ne cooling transition with high accuracy. Fig. 6 shows a comparison between the results presented here, and those of other groups using various experimental techniques. We note that earlier attempts [25–28], obtain a 4 MHz larger shift than more recent and accurate ones presented in this work and in [24]. It would thus be beneficial to conduct a high accuracy, ab initio calculation of this quantity, which as far as we know, does not exist in the literature.

To check our results with a different experimental system, we intend to conduct this measurement in our trap setup [29]. By measuring ^{21}Ne as well, it is also possible to improve the determination of the $^{20-22}\text{Ne}$ charge radii difference [30].

ACKNOWLEDGMENTS

This work was supported by the Israeli Science Foundation under ISF grant 139/15 and the Pazi Foundation. B.O. is supported by the Hoffman responsibility and leadership program.

-
- [1] M. Inguscio and L. Fallani. *Atomic Physics: Precise Measurements and Ultracold Matter*. OUP Oxford, 2013.
 - [2] T. Zelevinsky, D. Farkas, and G. Gabrielse. Precision measurement of the three 2^3P_J helium fine structure intervals. *Phys. Rev. Lett.*, 95:203001, Nov 2005.
 - [3] G.-P. Feng, X. Zheng, Y. R. Sun, and S.-M. Hu. Laser-spectroscopy measurement of the fine-structure splitting $2^3P_1 \sim 2^3P_2$ of ^4He . *Phys. Rev. A*, 91:030502, Mar 2015.
 - [4] A Marsman, M Horbatsch, and EA Hessels. Quantum interference effects in saturated absorption spectroscopy of $n=2$ triplet-helium fine structure. *Physical Review A*, 91(6):062506, 2015.
 - [5] E. Arimondo, M. Inguscio, and P. Violino. Experimental determinations of the hyperfine structure in the alkali atoms. *Rev. Mod. Phys.*, 49:31–75, Jan 1977.
 - [6] T. W. Hansch, M. D. Levenson, and A. L. Schawlow. Complete hyperfine structure of a molecular iodine line. *Phys. Rev. Lett.*, 26:946–949, Apr 1971.
 - [7] B W Petley, K Morris, and R E Shawyer. A saturated absorption spectroscopy measurement of the rydberg constant. *Journal of Physics B: Atomic and Molecular Physics*, 13(16):3099, 1980.
 - [8] L. Consolino, G. Giusfredi, P. De Natale, M. Inguscio, and P. Cancio. Optical frequency comb assisted laser system for multiplex precision spectroscopy. *Opt. Express*, 19(4):3155–3162, Feb 2011.
 - [9] Wim Vassen, Claude Cohen-Tannoudji, Michele Leduc, Denis Boiron, Christoph I. Westbrook, Andrew Truscott, Ken Baldwin, Gerhard Birkel, Pablo Cancio, and Marek Trippenbach. Cold and trapped metastable noble gases. *Rev. Mod. Phys.*, 84:175–210, Feb 2012.
 - [10] Masato Aketagawa, Takuya Yashiki, Shohei Kimura, and Tuan Quoc Binh. Free spectral range measurement of fabry-perot cavity using frequency modulation. *International Journal of Precision Engineering and Manufacturing*, 11(6):851–856, 2010.
 - [11] Wolfgang Demtröder. *Laser spectroscopy: basic concepts and instrumentation*. Springer Science & Business Media, 2013.
 - [12] P. G. Pappas, M. M. Burns, D. D. Hinshelwood, M. S. Feld, and D. E. Murnick. Saturation spectroscopy with laser optical pumping in atomic barium. *Phys. Rev. A*, 21:1955–1968, Jun 1980.

- [13] Eryn C. Cook, Paul J. Martin, Tobias L. Brown-Heft, Jeffrey C. Garman, and Daniel A. Steck. High passive-stability diode-laser design for use in atomic-physics experiments. *Review of Scientific Instruments*, 83(4), 2012.
- [14] JF Kelly and A Gallagher. Efficient electro-optic modulator for optical pumping of na beams. *Review of scientific instruments*, 58(4):563–566, 1987.
- [15] WW Macalpine and RO Schildknecht. Coaxial resonators with helical inner conductor. *Proceedings of the IRE*, 47(12):2099–2105, 1959.
- [16] C. Y. Chen, K. Bailey, Y. M. Li, T. P. O’Connor, Z.-T. Lu, X. Du, L. Young, and G. Winkler. Beam of metastable krypton atoms extracted from a rf-driven discharge. *Review of Scientific Instruments*, 72(1), 2001.
- [17] HO Di Rocco and A Cruzado. The voigt profile as a sum of a gaussian and a lorentzian functions, when the weight coefficient depends only on the widths ratio. *Acta Physica Polonica, A.*, 122(4), 2012.
- [18] S Andreon and Merrilee A Hurn. The scaling relation between richness and mass of galaxy clusters: a bayesian approach. *Monthly Notices of the Royal Astronomical Society*, 404(4):1922–1937, 2010.
- [19] Mauro Sereno. A bayesian approach to linear regression in astronomy. *Monthly Notices of the Royal Astronomical Society*, 455(2):2149–2162, 2016.
- [20] B. Ohayon, E. Wählin, and G. Ron. Characterization of a metastable neon beam extracted from a commercial rf ion source. *Journal of Instrumentation*, 10(03):P03009, 2015.
- [21] A. Marsman, M. Horbatsch, and E. A. Hessels. Shifts due to distant neighboring resonances for laser measurements of 2^3S_1 -to- 2^3P_J transitions of helium. *Phys. Rev. A*, 86:040501, Oct 2012.
- [22] P J Leo, D F T Mullanphy, G Peach, V Venturi, and I B Whittingham. Self-broadening of non-resonance neon lines. *Journal of Physics B: Atomic, Molecular and Optical Physics*, 29(20):4573, 1996.
- [23] R. Grimm and J. Mlynek. The effect of resonant light pressure in saturation spectroscopy. *Applied Physics B*, 49(3):179–189, 1989.
- [24] T. Feldker, J. Schutz, H. John, and G. Birkel. Magneto-optical trapping of bosonic and fermionic neon isotopes and their mixtures: isotope shift of the $3p^2 - 3d^3$ transition and hyperfine constants of the $3d^3$ state of ^{21}Ne . *The European Physical Journal D*, 65(1):257–262, 2011.
- [25] Lucile Julien, Michel Pinard, and Franck Laloe. Hyperfine structure and isotope shift of the 640.2 and 626.6 nm lines of neon. *Journal de Physique Lettres*, 41(20):479–482, 1980.
- [26] G. Guthohrlein and L. Windholz. *J. Opt. Res*, 2:171, 1994.
- [27] Gö. Basar, Gü. Basar, S. Büttgenbach, S. Kröger, and H. D. Kronfeldt. Parametric investigation of the isotope shift in odd configurations of ne i. *Zeitschrift für Physik D Atoms, Molecules and Clusters*, 39(4):283–289, 1997.
- [28] V. I. Odintsov. Isotopic Shift in the Spectrum of Neon. *Optics and Spectroscopy*, 18:205, March 1965.
- [29] Ben Ohayon and Guy Ron. Investigation of different magnetic field configurations using an electrical, modular zeeman slower. *Review of Scientific Instruments*, 86(10), 2015.
- [30] W. Geithner, T. Neff, G. Audi, K. Blaum, P. Delahaye, H. Feldmeier, S. George, C. Guénaut, F. Herfurth, A. Herlert, S. Kappertz, M. Keim, A. Kellerbauer, H.-J. Kluge, M. Kowalska, P. Lievens, D. Lunney, K. Marinova, R. Neugart, L. Schweikhard, S. Wilbert, and C. Yazidjian. Masses and charge radii of $^{17-22}\text{Ne}$ and the two-proton-halo candidate ^{17}Ne . *Phys. Rev. Lett.*, 101:252502, Dec 2008.